2-14-2014

Synthesis and Characterization of Bi-functional (ORR/OER) Nano-catalysts in Alkaline Media

Nalin Iris Andersen

Nalin Iris Andersen

Candidate

Nanoscience and Microsystems Engineering

Department

This thesis is approved, and it is acceptable in quality and form for publication:

Approved by the Thesis Committee:

Dr. Plamen Atanassov , Chairperson

Dr. Dimiter Petsev

Dr. Alexey Serov

Dr. Kateryna Artyushkova

SYNTHESIS AND CHARACTERIZATION OF BI-FUNCTIONAL ORR/OER NANO-CATALYSTS IN ALKALINE MEDIA

BY

NALIN IRIS ANDERSEN

B.S., CHEMICAL ENGINEERING, UNIVERSITY OF NEVADA, RENO, 2011

THESIS

Submitted in Partial Fulfillment of the
Requirements for the Degree of

Master of Science

Nanoscience and Microsystems Engineering

The University of New Mexico
Albuquerque, New Mexico

December 2013

ACKNOWLEDGEMENTS

I would like to thank, first and foremost, my advisor Dr. Plamen Atanassov for introducing me to the challenging field of catalysis. Through his guidance, supervision and knowledge, he has allowed me to develop my research with creative freedoms. I am thankful for the opportunity to have learned from his wealth of knowledge.

I consider it an honor to have had the pleasure of working with Dr. Alexey Serov, from which he has shown constant motivation and ingenious inspiration. His experimental advice and knowledge has led to innumerable and beneficial scientific discussions and laboratory findings.

I owe my deepest gratitude to my husband, Jason Andersen, for his encouragement, enthusiasm and utmost support.

SYNTHESIS AND CHARACTERIZATION OF BI-FUNCTIONAL ORR/OER NANO-CATALYSTS IN ALKALINE MEDIA

by

Nalin Iris Andersen

B.S., Chemical Engineering, University of Nevada, Reno, 2011
M.S., Nanoscience and Microsystems Engineering, University of New Mexico, 2013

ABSTRACT

The catalysts described in this thesis can be utilized in the systems that work by: storing energy, adding to the energy economy and directly converting chemical energy into electrical energy. This thesis presents the synthesis methods and characterization of three families of catalysts that are bi-functionally active, with high performance in the oxygen reduction reactions (ORR) and oxygen evolution reactions (OER) at the cathode and anode, respectively. All catalysts have been derived from transition metal oxides; an analysis on the synthesis and characterization has been conducted. The objectives are:

(i) explore synthetic approaches to achieving highly porous, phase pure nano-sized metal oxides in the form of spinels,

(ii) engineer functionalized carbon nanotubes (CNTs) that support metal oxide species and understand the intrinsic catalytic activity of different types of metal oxides deposited on them, and

(iii) combine data about the metal oxide species and synthesis methods from objectives (i) and (ii) to synthesize another set of catalysts and infer bi-functional catalyst properties.

To meet the first research objective, four synthetic approaches were explored to produce $CuCo_2O_4$ spinel catalysts. Based on their electrochemical activity, $CuCo_2O_4$ synthesized

by the sacrificial support method (SSM) was found superior compared to the other materials. The sacrificial support method involves the incorporation of oxide precursors onto the surface of fumed silica (or other sacrificial support), post-heat treatment, followed by removing silica in a manner that does not affect the chemical composition of the final catalyst. The resulting unsupported material has been found to be highly active in ORR with a half-wave potential of 0.80V and a limiting current density of -3.66 mA cm^{-2}. It was measured to have an onset potential of 1.52V versus the reversible hydrogen electrode (RHE) during the OER, which makes it a state-of-the-art bi-functional electrocatalyst.

The second research objective was achieved by the development of a modified SSM application to synthesize functionalized CNTs. Furthermore, various metal oxides were deposited onto the CNT surfaces (MO_x/CNT) with a loading of 50wt%, resulting in catalysts where the CNTs act as durable, highly electronic conductive carbon supports. All catalysts in this series have high activity in the OER and ORR cycles. It was found that the 25wt% Ni + 25wt% Mn/CNT catalyst was the best performer for the OER with an onset potential of 1.41V versus RHE; the best ORR catalyst is the 50wt% MnO_2/CNT catalyst with a half wave potential of 0.84V at a current density of -2.1 mA cm^{-2}. Both materials show high stability and durability in ORR and OER conditions.

The third research objective was to synthesize catalysts by combining the methods that yielded the best catalysts from the first two research objectives. Two new sets of catalysts were derived and the catalysts were electrochemically analyzed. For the first set of catalysts, the SSM technique was used to evaluate Ni and Mn oxide species; the second set of catalysts resulted from the deposition of Cu and Co onto CNTs. Although this new

series of catalysts did not perform as well as those synthesized by the methods in the first two research objectives, they do provide an understanding of the electrochemical effects of combining multiple transition metal oxide species.

TABLE OF CONTENTS

CHAPTER 1 INTRODUCTION

1.1 Background

The world needs portable and distributed energy storage and conversion devices to support an emerging non-hydrocarbon fuel economy. Catalysts and their design are central to these devices, which are intrinsically safe to provide adequate power where and when it is needed. These devices (*e.g.* fuel cells, electrolyzers and batteries) can be applied to a variety of applications, whether that's in a car driving down the road, at remote command and control centers in military settings, smart grid energy storage at off-grid sites or in a child's toy. Presently, platinum-group metals (PGM) are used in these chemical energy conversion systems [1-2]. Much research has gone into the design and utilization of these materials, with variations on multiple parameters to increase their efficiency. Thus, the resulting catalytic properties of PGM-based materials establish the benchmarks of the catalyst field; however, these materials are scarce, expensive, and the mining resources are located in politically unstable countries. The prime cost of these particular catalysts has driven the high price of the final devices, inhibiting wide-spread commercial viability. Accordingly, it is desired to create economical and functional substitutes to PGM-based materials derived from inexpensive materials such as transition metal oxides.

1.2 Clean Energy Production, Storage and Conversion

Energy management including production, storage and conversion is fundamental to an efficient economy. Energy production is achieved through fuel cell application, energy storage is achieved in part through batteries, and energy conversion occurs by application of electrolyzers. Clean energy management can be accomplished by employment of catalysts tailored to their applications, which produce environmentally benign

byproducts. These catalysts facilitate two electrochemical mechanisms: oxygen reduction reactions (ORR) at the cathode and oxygen evolution reactions (OER) at the anode, both of which are at the foundation of electrically powered energy systems. Figure 1 shows a comparison of three technologies: an alkaline electrolyzer [3], a Li-air battery [4] and an alkaline fuel cell [5], (from left to right). These devices function using alkaline environments, found to have lower overpotential losses than in acidic media [6]. The design of such catalysts will potentially contribute to the building blocks of a clean energy cycle.

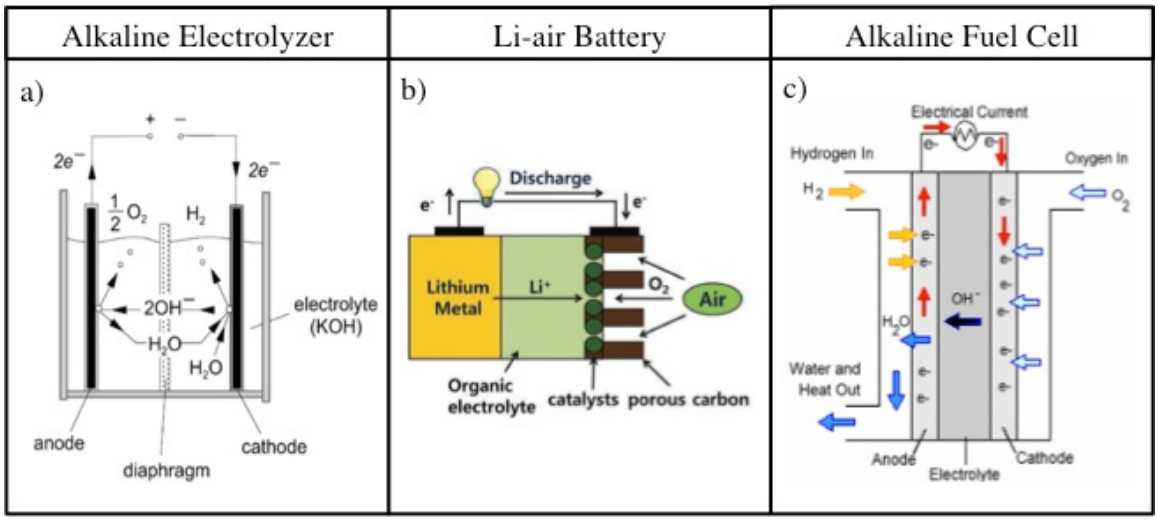

Figure 1. a) alkaline electrolyzer, b) Li-air battery and c) alkaline fuel cell

Alkaline electrolyzers work by splitting water into hydrogen and oxygen; this is achieved by passing a current with minimum electric voltage to the two electrodes. This minimum voltage can be determined from Gibbs energy for splitting water. The potassium and hydroxide ions in the electrolyte facilitate the ionic transport [3]. The chemical reactions that take place in an alkaline electrolyzer are shown below:

Cathode: $2H_2O + 2e^- \rightarrow H_2 + 2OH^-$

Anode: $2OH^- \rightarrow \frac{1}{2}O_2 + H_2O + 2e^-$

Li-air batteries have open cell structures because they utilize oxygen from the air as their cathodes and use Li metal as the anode material. In the reaction mechanisms within a Li-air battery, Li^+ ions travel through the electrolyte and reacts with oxide ions at the air cathode forming Li_2O_2 precipitate. The cathodic reaction mechanisms were introduced by Abraham, *et al*. [7] and Ogasawara *et al*. introduced the anodic mechanism based on *ex situ* powder x-ray diffraction (XRD) and *in situ* mass spectroscopy [8]. These mechanisms are based on the Li-air battery technology utilizing a non-aqueous electrolyte [4]. System reactions are shown below:

Cathode: $2Li + O_2 \rightarrow Li_2O_2$

$4Li + O2 \rightarrow 2Li_2O$

Anode: $H_2 + 2OH^- \rightarrow 2H_{2O} + 2e^-$

Alkaline fuel cells produce electricity and water. They can operate at temperatures ranging from room temperature to 80°C. Alkaline fuel cells have been shown to have efficiencies as high as 60% in space applications like the NASA Apollo Mission, due to the rapid chemical reaction rates within the cells [9]. This type of fuel cell uses potassium hydroxide solution as the electrolyte and can use non-PGM catalysts to push the anodic and cathodic reactions forward as shown below [5].

Cathode: $O_2 + 2H_2O + 4e^- \rightarrow 4OH^-$

Anode: $H_2 + 2OH^- \rightarrow 2H_2O + 2e^-$

Catalyst design, synthesis and integration into these systems are crucial to building, increasing efficiencies, and expanding the application of fuel cells, batteries, and related devices. A material produced to perform well in alkaline media can function in any of the systems shown in Figure 1, if they have been optimized to operate in compatible chemical environments. The purpose of this research is to explore ways of synthesizing such catalysts.

1.3 Research Objectives

A considerable amount of catalyst design is theorized and modeled mathematically. In contrast, the main objective of this research is to discover and successfully synthesize bi-functional catalysts at the laboratory scale, with possible scale-up to tens of grams. The term, "bi-functional" means that these are catalysts that perform electrochemically in reactions of oxygen reduction and oxygen evolution, which increases the flexibility of their application. The objectives are to synthesize and characterize three families of catalysts:

(i) $CuCo_2O_4$ spinel catalysts by different synthetic approaches,

(ii) metal oxides supported on CNT (MO_x/CNT) catalysts and

(iii) combining the metal oxides, CNTs and synthetic approaches of the best performing catalysts from (i) and (ii).

CHAPTER 2 CATALYST SYNTHESIS AND CHARACTERIZATION

The research followed the path of: (i) design, (ii) synthesis and (iii) characterization. Design includes selecting promising candidates based on literature review and in some cases, targeting the morphology. Synthesis methods are selected as a function of the precursors chosen and standard chemical laboratory practices, with modifications to achieve the highest performance in both ORR and OER. Characterization is achieved through standard laboratory techniques and has two parts: physical and electrochemical.

2.1 Catalyst Design

The reactions at the catalytic interfaces determine the efficiency of energy devices. The accessibility of a catalyst's active sites to the fuel of choice and successful removal of products from them is a function of the catalyst's intrinsic chemical and physical properties. In the synthesis of catalysts, there are several variable components that must be tuned to obtain highly electrochemically active materials. Factors that influence the final performance of energy conversion systems are: surface area and morphology of the catalyst, the distribution of active sites on its surfaces, electrical conductivity and the design of the electrode surfaces. This optimization of the gas and water transport within a chemical conversion system will lead to the best catalyst for anode water oxidation reaction rates and cathodic oxygen reduction reactions. The scope of this research is to focus on the synthesis of active catalysts, evaluate their physical and electrochemical properties, and to formulate structure-to-properties relationships.

2.2 Catalyst Synthesis

In the design and development of an active catalyst, the focus of this research is on the synthesis of such materials. Promising research and innovation in catalyst design has led to a variety of synthesis approaches. Non-trivial challenges that must be overcome include: morphological control, catalyst durability and production scalability.

2.2.1 Morphology

A catalyst's function is dependent on its morphology and intrinsic chemical properties. Morphological control includes consistent porosity, surface area and overall physical characteristics. In the example of CNT synthesis, the morphology properties can vary substantially. The CNTs can be altered in terms of thickness, shape, number of walls and purity (amount of amorphous carbon). The CNTs can grow in the shape of corkscrews given the appropriate precursors. Furthermore, the diameter of their walls can vary depending on the precursor seeds chosen. In contrast, the $CuCo_2O_4$ spinel synthesized via SSM yielded spherical catalysts. The amount of sacrificial support used in all catalysts synthesized influences their surface areas. Temperature effects and introduction of chemicals incorporated in the synthesis of the catalysts must be tuned to yield materials with the highest amount of available active sites. In the bodies of work presented here, these challenges have been explored in great depth and have been overcome to achieve overall structural control of the acquired catalytic frameworks.

2.2.2 Durability

A catalyst's durability dictates whether or not it will reliably function in a commercial device under expected operating conditions. During a device's lifetime, the catalysts get cycled numerous times and their activity decreases. Reducing this degradation rate is

related to a catalyst's chemical and physical components. First, this is a chemical issue because the ORR and OER are functions of the consumption and evolution of the appropriate gases at the active sites of a catalyst. Activity losses can occur when unwanted side reactions are present - primarily the formation of H_2O_2 or a reaction of the electrolyte with CO_2 from the air, which can cause a drop of performance. Second, this is a physical issue because during the device's operational lifetime, the catalytic infrastructure is prone to degradation. This decreases the number of active sites and contaminates the electrolyte. It is well known that the addition of carbon to catalysts increases their conductivity; however, this carbon is typically amorphous and rapidly degrades during the anodic sweeps. In the design of the 50wt% MO_x/CNT catalysts, this durability issue was of primary concern. With a rational fabrication model, these problems were addressed and the 50wt% NiO/CNT catalyst's performance substantially increased during a 1000-cycle durability test.

2.2.3 Scalability

One of the most relevant challenges to catalyst commercialization is scalability of the production processes. Bulk production is rarely linear and an intriguing problem. This is handled on a case-by-case basis and is primarily solved by careful and iterativeexperimental design. The preparation method for the functionalized CNTs was based on modifying the SSM technique, which offers control over the carbon nanotube morphology and level of functionalization. The production rate can be increased to several kilograms per batch, which will substantially decrease the price of CNTs (~2000USD per kilogram in 2013). The $CuCo_2O_4$ spinel catalyst fabricated using the modified spray pyrolysis method has been proven to yield large batches with uniform spherical structural and electrochemical properties by fine-

tuning the required atomization of the materials and temperature sequencing.

2.3 Physical Characterization

Four physical characteristics were measured as explained below:

- The physical morphologies of the reported catalysts from Chapters 3 and 4 have been analyzed with Scanning Electron Microscopy (SEM, Hitachi S-5200) and Transition Electron Microscopy (TEM, JEOL 2010 EX HREM).
- Chemical components within the catalysts were determined using X-ray Diffraction (XRD, Scintag Pad V, Cu anode).
- Elemental compositions within the catalysts were measured using X-ray Photoelectron Spectroscopy (XPS, Kratos Axis DLD Ultra X-ray photoelectron spectrometer using an Al Kα source monochromatic operating at 150W with no charge compensation).
- Catalyst surface areas have been comprehensively characterized by the Brunauer-Emmett-Teller method (BET).

2.4 Electrochemical Characterization

Catalytic activity was measured using a Rotating Disc Electrode (RDE) experiment, following hydrodynamic voltammetry theory. The results from an electrochemical experiment are influenced by convection of the solution surrounding the electrode. By rotating the electrode in solution, one is able to achieve laminar flow adjacent to the electrode surface. For the scope of this thesis, all materials were tested by rotating the electrode at 1600 RPM. This allows half reactions to be successfully measured by

applying varying potentials to the electrode. When a positive potential is applied, the catalyst's molecules are oxidized and electrons are getting removed from the molecules or ions in the electrolyte, leaving the solution and entering the electrode. In the same way, when a negative potential is applied, the catalyst is reduced and electrons are added to the molecules or ions leaving the electrode and this is a cathodic current. As the electrode potential changes from an initial to final value at a constant rate, the current can be measured [10].

For this thesis, all catalysts were measured in 1.0M KOH, prepared from deionized water and KOH pellets (99.99%, Sigma-Aldrich). The reference Hg/HgO electrode corresponds to a reversible hydrogen electrode (RHE) of 0.926 at 25°C. The counter electrode used was a Pt wire. The catalytic inks were prepared by mixing the catalyst powder with an optimized amount of Nafion™ ionomer with an IPA/H_2O solution. The Nafion™ is used as a binder for the catalyst as well as a proton pathway for the ORR and OER. The inks were sonicated using an ultrasound probe to ensure homogeneity and the catalysts were loaded onto a Pine Instrument electrode in the amount of either 0.2 mg cm^{-2} or 0.4 mg cm^{-2} [11-12].

CHAPTER 3 RESEARCH OBJECTIVE 1: SPINEL CATALYSIS

Syntheses of spinel catalysts were conducted to explore different transition metal oxides with high catalytic activity. Experimentally, perovskites, spinels and pure oxides were examined electrochemically using variations of the following 3d metals: Fe, Mn, Ni, Co and Cu (*e.g*. $FeCoO_3$, $MnNiO_3$, $CuMn_2O_4$, $MnFe_2O_4$, CuO, NiO, etc.) with variation of numerous synthetic approaches. This resulted in the findings that the sacrificially supported $CuCo_2O_4$ spinel catalyst was the most active and showed the best phase purity.

3.1 Abstract

A set of $CuCo_2O_4$ spinel catalysts was synthesized using four synthetic approaches. These materials show bi-functional behavior and the best performer of the series was developed using a sacrificial support method (SSM). With this technique, the SSM-derived spinel was found to be the most phase-pure as well as the most electrochemically active. The SSM-$CuCo_2O_4$ catalyst has a half-wave potential of 0.80V at the current density of -1.5 mA cm^{-2} and an onset potential of 1.52V during the OER.

3.2 Introduction

The development of fuel cells, electrolyzers and Li-air batteries can all benefit from efficient bi-functional catalysts. The objective of this study is to explore the influence of four synthesis methods on the final electrochemical performance of bi-functional catalysts: 1) pore forming (PF), 2) sol-gel (SG), 3) spray pyrolysis (SP), and 4) sacrificial support method (SSM). La-containing perovskite oxides [13-15] and spinels [16-17] have been reported in literature; however, the synthesis of a bi-functional $CuCo_2O_4$ spinel has not been evaluated to our best knowledge. The criteria of determining the best synthetic

methods were: scalability, reproducibility and electrochemical activity. All catalysts must also be stable in alkaline media. The results of the four synthesis methods have been analyzed and resulting catalysts have been characterized.

3.3 Synthesis

$CuCo_2O_4$-PF synthesis method: Dissolved $Cu(NO_3)_2$ and $Co(NO_3)_2$ (99%, Sigma-Aldrich) were mixed with 2g $C_{12}H_{22}O_{11}$ (sucrose) and 2g CH_4N_2O (urea). A colloidal suspension of fumed silica (Cabot, EH-5) was added to the solution. This material is dried in air at 85°C for 24 hours, ground with agate mortar and pestle, and placed in a furnace. The powder is pyrolyzed in a N_2 atmosphere at 300°C for 5 minutes then 550°C for 120 minutes. It is then exposed to an oxygen heat treatment at 300°C for 5 minutes then 500°C for 120 minutes. All gases used are ultra high-grade purity. The material was removed from the furnace, leached with 6M KOH (Sigma-Aldrich) for 24 hours and centrifuged. This leaching process was conducted three times. This enabled total removal of silica from the material. The material was then washed to reach a neutral pH and then dried.

$CuCo_2O_4$-SG synthesis method: Dissolved $Cu(NO_3)_2$, $Co(NO_3)_2$ and excess $NaHCO_3$ (99%, Sigma-Aldrich) were centrifuged. The precipitate was dried and calcined at 550°C for 180 minutes.

$CuCo_2O_4$-SP synthesis method: Dissolved $Cu(NO_3)_2$ and $Co(NO_3)_2$ (99%, Sigma-Aldrich) were mixed with a colloidal suspension of fumed silica (Cabot, EH-5). The solution was ultrasonically atomized and heat treated in a furnace at 275°C with N_2 as the

carrier gas with a flow rate of 1L min^{-1}. The material was deposited onto filter paper, gently scraped off and calcined at 500°C for 180 minutes.

$CuCo_2O_4$-SSM synthesis method: Dissolved $Cu(NO_3)_2$ and $Co(NO_3)_2$ (99%, Sigma-Aldrich) were mixed with a colloidal suspension of fumed silica (Cabot, EH-5). The solution is dried in air at 85°C for 24 hours, ground with agate mortar and pestle, and placed in a furnace. The powder is calcined at 500°C for 180 minutes, leached with 6M KOH (Sigma-Aldrich) for 24 hours and centrifuged. The materials were washed to reach a neutral pH and dried.

3.4 Results and Discussion

Four catalysts were synthesized in this study, in which $CuCo_2O_4$ was formed. The four synthesis methods are first discussed relative to controlling catalyst morphology described here. This is followed by a discussion of the qualitative character of the resulting catalysts.

The pore-forming (PF) method utilized the addition of urea with the goal of forming appropriately sized pores within the catalytic matrix. If the catalyst's surface area is high but the pores are too small, the pores can become inaccessible. This inhibits the fuel from reaching the catalyst's active sites leading to poor mass activity. If the catalyst has low catalytic surface area, the active sites are not exposed to the fuel. The surface area of this catalyst is 9 m^2 g^{-1}. The pore-forming method was an opportunity to understand the effects of the addition of urea into the catalyst to optimize the relationship between the catalyst's surface area and its pore sizes.

The sol-gel (SG) method involved reacting sodium bicarbonate with the Cu and Co nitrate precursors to form copper and cobalt hydrated sols: $M_x^I M_y^{II} O_z \cdot H_2O$ (where M = Co and Cu). The precipitate that formed was heat treated in an air atmosphere. This method was designed to create a spinel that possesses high surface area from a continuous porous network inside the catalyst. The surface area of this catalyst is 22 m^2g^{-1}.

The spray pyrolysis SP method is based on the solidification of aerosol droplets of precursors transported through a pre-heated furnace. The atomization of copper and cobalt nitrates in solution was achieved by using a high-energy ultrasound generator. Spherical solid particles formed during solvent evaporation were collected on the Teflon™ filter at the outlet of the furnace followed by additional post processing at 500°C in air. This catalyst has a surface area of 10 m^2 g^{-1} and this technique was chosen to create a controlled-morphology catalyst to further understand the relationship between a catalyst's physical and electrochemical properties.

The sacrificial support method (SSM) was developed at the University of New Mexico for the purpose of designing materials with high surface area and controlled morphology to maximize the density of catalytic active sites. The surface area of this catalyst is the highest among this series at 40 m^2 g^{-1}. The nitrate precursors were mixed with fumed silica, heat treated, followed by leaching the silica. The $CuCo_2O_4$ created by SSM resulted in the most phase-pure material. X-ray diffraction was used to confirm phase compositions of these four materials as shown in Figure 2. The "★" indicates the $CuCo_2O_4$ peaks and the "❖" indicates residual CuO formation.

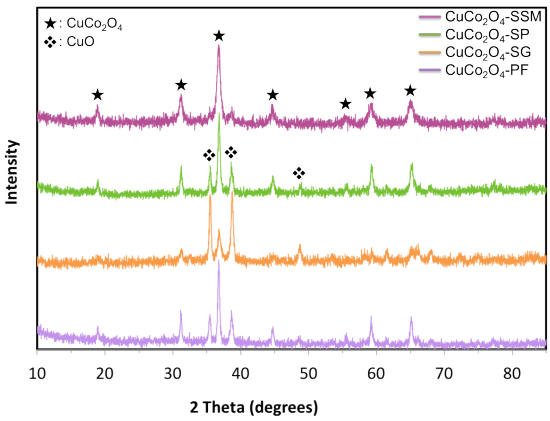

Figure 2. XRD data for $CuCo_2O_4$ catalysts prepared by a) pore-forming method (PF), b) sol-gel method (SG), c) spray pyrolysis (SP) and d) sacrificial support method (SSM). Condition: T=550°C, t=3h.

To compare the morphological properties of the catalysts, SEM and TEM were used and these images are shown in Figure 3.

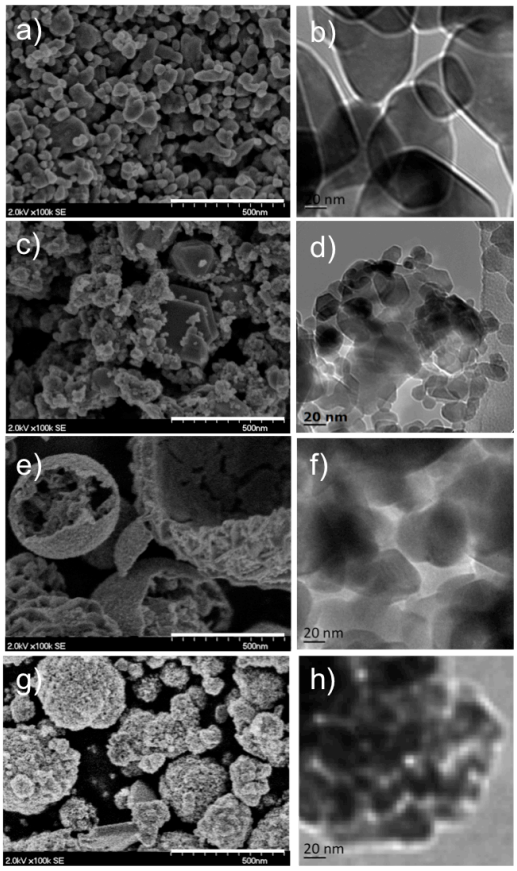

Figure 3. SEM (left column) and TEM (right column) images of $CuCo_2O_4$ catalysts prepared by a) and b) pore-forming method (PF), c) and d) sol-gel method (SG), e) and f) spray pyrolysis (SP) and g) and h) sacrificial support method (SSM).

Varying the synthesis techniques yielded very different morphological characteristics despite having similar chemical properties. The $CuCo_2O_4$-PF catalyst has smooth agglomerations ranging in size from 10-250nm. The $CuCo_2O_4$-SG catalyst has both smooth and rough surfaces ranging in size from 80nm-140nm with some porous areas. The $CuCo_2O_4$-SP catalyst is spherical in shape, with spheres as large as 2μm. It has been observed that some spheres are quite hollow as shown in Figure 3e, and in some cases, smaller spheres were found embedded into the larger spheres. From the TEM image in Figure 3f, we can deduce that the spheres are solid and do not have a uniform outer film, but are agglomerates of the $CuCo_2O_4$ nanoparticles. The $CuCo_2O_4$-SSM catalyst is spherical in shape as well. As in the $CuCo_2O_4$-SP, this catalyst contained spheres that ranged in size from 150nm-1.5μm as can be seen in Figure 3g. The $CuCo_2O_4$-SSM catalyst is electronically dense, but the spherical shape can be seen again in Figure 3h.

The electrochemical activities of the catalysts are shown in Figure 4. These results show that the $CuCo_2O_4$-SSM material is the best performer among the four catalysts compared. It has a half-wave potential of 0.80V at a current density of -1.8 mA cm^{-2} and an onset potential of 1.52V versus RHE during the OER.

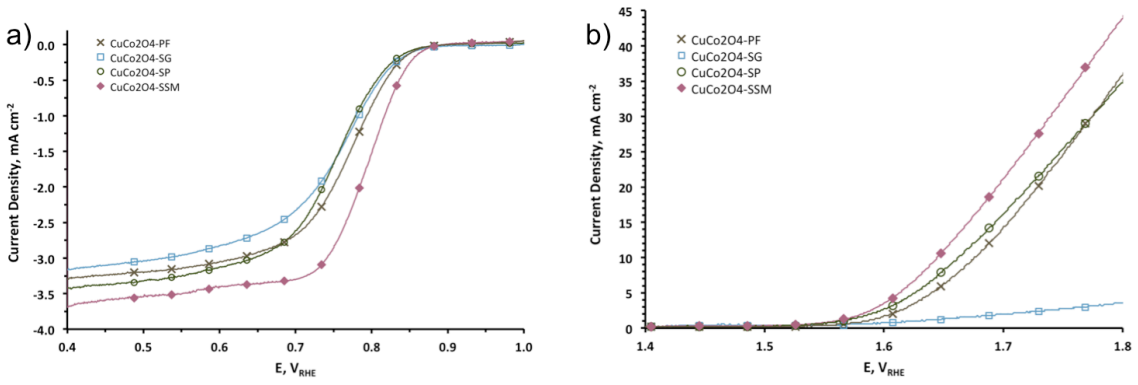

Figure 4. Electrochemical data on $CuCo_2O_4$ catalysts: (a) RDE in oxygen reduction, (b) RDE in oxygen evolution. Conditions: catalyst loading is 200μg cm^{-2}, 1M KOH, 1600RPM, 10mV s^{-1}.

An electronic conductivity test was performed in which each catalyst was formed into a pellet of equal size and its electrical resistance was measured. The $CuCo_2O_4$-SSM catalyst showed the least resistance of <1Ω. The other three catalysts had resistivities between 400Ω – 400MΩ. The poorest performer (as measured by current density) of this series is the $CuCo_2O_4$-SG catalyst. This catalyst was compared to CuO-SSM, which was synthesized in the same manner as the $CuCo_2O_4$-SSM catalyst. The materials were compared to CuO-SSM, because CuO is the residual species after synthesis. The SSM method was chosen to make the catalyst because it produces the most phase pure materials as shown in Figure 2. The resistance of the CuO-SSM catalyst was 400kΩ so any traces of CuO in the catalysts will reduce their conductivity. The electrochemical comparisons of these catalysts are shown in Figure 5.

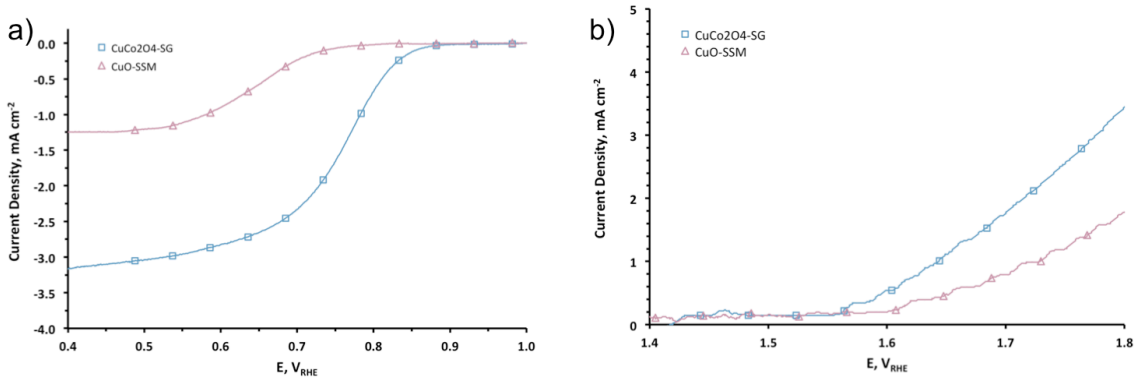

Figure 5. Electrochemical data on $CuCo_2O_4$-SG and CuO-SSM catalysts: (a) ORR and (b) OER. Conditions: catalyst loading is 200μg cm^{-2}, 1M KOH, 1600RPM, 10mV s^{-1}.

The results from the electrochemical studies and the XRD patterns indicate that traces of CuO within the catalyst decreases catalytic activity. This leads to the conclusion that a $CuCo_2O_4$ material can be utilized in energy systems; however, it is imperative that it is phase pure. Furthermore, it can be deduced that both Cu and Co components are necessary for the ORR and OER. From Figure 4, it is likely that the different components within $CuCo_2O_4$ are responsible for the catalyst's activity due to the different chemical

mechanisms that must be taking place. The material's electrically dense spherical morphology may also play a role in its activity.

3.5 Conclusions

By differing catalyst synthesis methods, materials are formed that can have very similar chemical properties (Figure 2), different physical properties (Figure 3) and varying electrochemical results (Figure 4). This research provides some insight to some of the properties necessary for a successful bi-functional catalyst. The materials formed are all unsupported and easy to synthesize. Scale-up of the products is possible with the techniques described. The electrochemical comparison of the $CuCo_2O_4$ catalyst to the CuO (Figure 5) shows the importance of the role of the Co-oxide specie, and particularly that the spinel structure is electrochemically active.

CHAPTER 4 RESEARCH OBJECTIVE 2: CARBON-HYBRID CATALYSIS

The motivation for this research objective is to explore carbon-hybrid catalysts that are easy to synthesize and are durable. Typically, CNTs are hydrophobic and chemically inhibit any type of oxide-containing deposition. A synthetic method for developing functionalized CNTs has been used, in which it is assumed the oxophilic functional groups are: carbonyl (-C=O), hydroxyl (-OH) and carboxyl (-COOH) on the surfaces of the nanotubes. It is also an objective to suppress the parasitic side reaction that results from growing CNTs where amorphous carbon is formed. Amorphous carbon is unstable under OER conditions and decreases the catalyst's surface area while preventing uniform distribution of the oxide phase. This research is notable because the state-of-the-art formation of these specialized CNTs proves to be durable during the OER cycles with minimal amorphous carbon and actually increases in activity the longer it was tested. The work is described in the following publication: (Andersen, N., Serov, A., Atanassov, P. *ChemElectroChem*. Submitted: October 2013).

4.1 Abstract

A series of catalysts were synthesized by deposition of transition metal oxides (MnO_2, CoO, NiO, etc.) on CNTs for bi-functional catalysis in alkaline media. The metal oxides were dispersed onto functionalized CNTs by an improved impregnation method. The novel synthetic approach allowed preparing functionalized CNTs and evenly dispersing metal oxides on the surface of carbon-nanotubes. These catalysts are stable in alkaline media under experimental conditions and have high bi-functional electrocatalytic activity. From this series of catalysts, the most active catalyst for ORR is the 50wt% MnO_2/CNT catalyst with a half wave potential of 0.84 V at the current density of -2.1 mA cm^{-2} and an

onset of 1.53V versus RHE. The most active for OER is the 25wt% Ni + 25wt% Mn/CNT catalyst with an onset potential of 1.41V versus RHE. A series of catalysts were synthesized by deposition of transition metal oxides (MnO_2, CoO, NiO, etc.) on CNTs for bi-functional catalysis in alkaline media. The metal oxides were dispersed onto functionalized CNTs by an improved impregnation method. The novel synthetic approach allowed preparing functionalized CNTs and evenly dispersing metal oxides on the surface of carbon-nanotubes.

4.2 Introduction

The majority of our world's vehicles are dependent on petroleum-derived fuels. The craving for these fuels has led to political unrest, wars, poverty and mass pollution. Furthermore, the conversion of chemical potential energy into kinetic energy from these fuels is quite low. Fuel cell technology has been extensively researched to address these issues. Fundamentally, these fuel cells are driven by electrochemical kinetics and intrinsic kinetics at the catalyst layer. Recently, interest to bi-functional catalysts has significantly grown from manufacturers of metal-air batteries, electrolyzers and fuel cells. By placing PGM catalysts these on commercial carbon supports that have high surface area, it enhances their activity [18]. The most active OER catalysts are made from IrO_2. The main drawback and need for more catalyst research is the incredibly high cost and low abundance of both Pt-group elements.

Bi-functional catalysts have been explored by other researchers in the past in which PGM catalysts were synthesized. Yi-Chun Lu, *et al*. studied 40wt% PtAu/C where the carbon source was Vulcan (XC-72) for use in Li-Air batteries [19]. Previously, non-PGM bi-functional materials have also been explored. Namely, a $La_{0.6}Ca_{0.4}CoO_3$ catalyst was

studied by Youichi Shimizu, *et al*. in 1990 [20], O. Haas, *et al*. in 2002 [21] and Xianyou Wang, *et al*. in 2003 [22] and showed good activity in ORR/OER. More recently, the mixed metal oxide $Sm_{0.5}Sr_{0.5}CoO_{3-x}$ by S. Velraj and J.H. Zhu has shown improved cyclic life in comparison to the $La_{0.6}Ca_{0.4}CoO_3$ catalyst and was dispersed on Vulcan carbon for the cathodic cycles [23]. A $LaNiO_3$ center, supporting nitrogen-doped CNTs was synthesized and studied by Zhu Chen, *et al*. [24] in which high performance was reported for OER and ORR. Deposition of copper nanoparticles onto the surfaces of oxides was present in the works of Wei Yang, *et al*. in which $Sr_{0.95}Ce_{0.05}CoO_{3-x}$ was made [25] and flowerlike Co_3O_4 microspheres were created [26], which were both loaded with Cu nanoparticles with stable bi-functional properties. Anchored $La_{0.5}Ce_{0.5}Fe_{0.5}Mn_{0.5}O_3$ onto graphene sheets was found to be electrochemically stable and retained 70% efficiency by Lixin Wang, *et al*. [27]. Yunlong Zhao, *et al*. made mesoporous perovskite $La_{0.5}Sr_{0.5}CoO_{2.91}$ nanowires, found to have high performance, low peak-up potential and high limiting diffusion current [28].

A family of catalysts have been derived that are stable in alkaline media, have large surface area, are easy to synthesize, can be produced at lower cost from abundant transition metals and still have high bi-functional electrocatalytic activity. In addition, an understanding of the structure-to-properties relationships was a subject of the research. Presented is a new method of functionalized CNT preparation based on the SSM developed at UNM [12, 29-37], synthesis, characterization and electrocatalytic activity of MO_x/CNT hybrid catalysts in ORR and OER.

4.3 Synthesis

The CNTs were synthesized by a conversion of C_2H_4 on Fe nanoparticles using the sacrificial support method. $Fe(NO_3)_3$ was mixed with a colloidal suspension of a silica sacrificial support (Cab-O-Sil® EH-5, 380m^2 g^{-1}), dried and ball milled for 4 hours at 450 RPM (Across International PQ-N04 Planetary Ball Mill) and placed in a furnace. The powder sample was exposed to a heat treatment at 500°C in a H_2 atmosphere for 30 minutes, 760°C in a C_2H_4 atmosphere for 60 minutes and 900°C under an NH_3 atmosphere for 60 minutes. The results from the XPS analysis confirms the presence of nitrogen defects on the surface of the nanotubes from the introduction of ammonia, which in turn, acts as anchors for the oxides. All gases used were ultra high-grade purity. The material was removed from the furnace, leached with HF and washed to reach a neutral pH [38-42]. Concentrated nitric acid is introduced, resulting in CNTs with no amorphous carbon. An impregnation method was then utilized in which liquid transition metal nitrates (99.98%, Sigma-Aldrich) were deposited on the CNT powder to yield 50wt% metal oxides, referred to as MO_x, deposited on the CNTs. The resulting material was dried overnight in the presence of oxygen at 85°C leaving a metal salt catalyst. After drying, the MO_x/CNTs (M: Fe, Mn, Ni, Co, Cu) were calcined at 350°C for 120 minutes. This synthesis method was chosen to keep the metal oxide agglomerations as small as possible to allow for maximum active sites per catalyst mass.

4.4 Results and Discussion

The novelty in the design of this series of catalysts lies within the synthesis of the CNTs, which allowed for deposition of metal oxide particles onto the graphitic surfaces, forming bi-functional catalysts. The surfaces of standard CNTs are hydrophobic, which inhibit the

deposition of metal oxides and promote the oxides to agglomerate. Here, the CNTs were produced using the SSM method in which a metal oxide precursor is dispersed in a colloidal suspension of a sacrificial support, then is decomposed and reduces to form crystallite seeds. The size of these metal seeds dictates the outer diameter of the CNTs. Upon the utilization of a carbon source to begin the growth of the CNTs on the aforementioned crystallite seeds, amorphous carbon is formed in a parasitic side reaction. Ammonia is introduced with the advantage of chemically etching some of the amorphous carbon as well as promoting the generation of nitrogen defects on the CNTs surfaces. A chemical etchant is used to leach the sacrificial support and any unreacted crystallite formations. To combat the issue of remaining amorphous carbon, nitric acid is used which simultaneously creates oxophilic groups on the CNT surfaces. This, in turn, successfully yields CNTs with the ability to support functional groups.

Five catalysts were synthesized and analyzed, in which individual transition metal-salt precursors were deposited onto the functionalized CNTs. The deposition percentage of transition metal oxides onto the CNT surfaces is 50wt%. The catalysts are: 50wt% MO_x/CNT (M: Co, Mn, Fe, Cu, Ni). X-ray diffraction was used to characterize the catalysts. The XRD results of the two electrochemically best catalysts, 50wt% MnO_2/CNT and 50wt% NiO/CNT are shown in Figure 6, while the XRD results of the 50wt% Co_3O_4/CNT and 50wt% CuO/CNT catalysts are shown in Section 4.6, Figure S1.

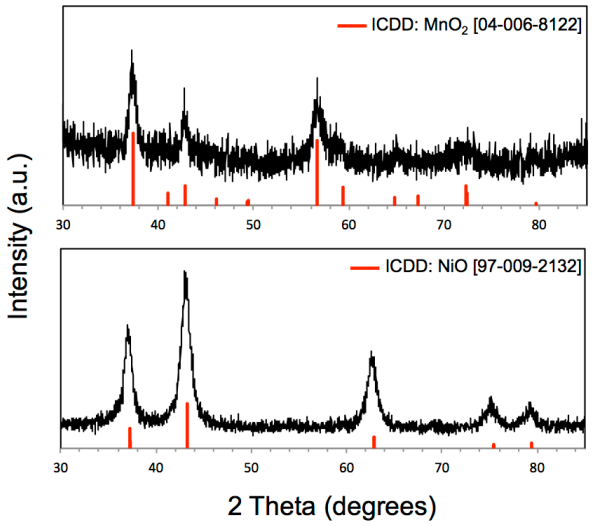

Figure 6. XRD data for a) 50wt% MnO_2/CNT and b) 50wt% NiO/CNT

The morphological properties of the catalysts were examined by SEM and TEM methods. The SEM images serve the purpose of understanding the morphology of the catalysts on a larger scale. In Figure 7, the SEM image scale bar is 1.00 μm. According to the following descriptions, the term, "particle," will be used to describe the metal oxide deposited on the CNTs. Varying particle size distributions and configurations of the catalysts can be examined. From the TEM images, it is shown that transition metal oxide nanoparticles have been successfully deposited onto the CNTs. The TEM images have a scale bar equivalent to 50 nm.

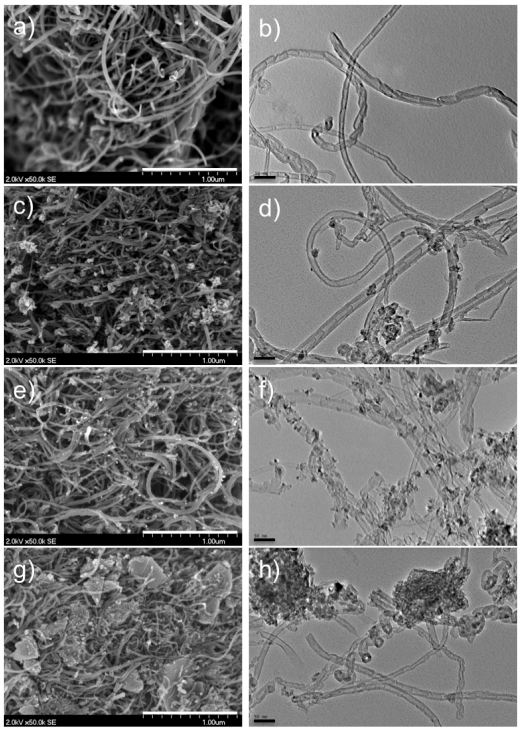

Figure 7. SEM (left column) and TEM (right column) images of: a) and b) bare CNTs, c) and d) 50wt% MnO_2/CNT, e) and f) 50wt% NiO/CNT and g) and h) 50wt% Fe_xO_y/CNT.

The technique of synthesizing CNTs with functionalized surfaces allowed for minimal amorphous carbon formation. Visually, this lack of amorphous carbon can be seen in the SEM image of the bare CNTs in Figure 7a. The bare CNTs used to template the metal oxides have a surface area of 120 m^2g^{-1} and are also shown via TEM in Figure 7b. The CNTs have a diameter averaging from 40 - 60nm, indicative of the size of the Fe crystallites formed during the H_2 purging phase of the synthesis, suggesting these are multi-walled carbon nanotubes.

The 50wt% MnO_2/CNT catalyst has a surface area of 83 m^2g^{-1} and features a large size distribution of oxide particles deposited onto the CNTs. It possesses a mixture of small 8nm nanoparticles up to larger, porous agglomerations approximately 500nm in size and is shown in Figures 7c and d. The 50wt% NiO/CNT catalyst has evenly distributed oxide

on the nanotube surfaces with very little agglomeration and a surface area of 134 m^2g^{-1}. Furthermore, the nanosized particles have a small size distribution of about 5nm and is shown in Figures 7e and f. The 50wt% Fe_xO_y/CNT catalyst has a surface area of 136 m^2g^{-1} and was electrochemically outperformed by all others in this series. Its features include nanotubes wrapped around shattered, crystalline oxide shards up to 800nm in size and is shown in Figures 7g and h. The 50wt% Co_3O_4/CNT catalyst has particle sizes from 25-200nm and surface area of 60 m^2g^{-1} with minimal agglomeration and is shown in Section 4.6, Figures S2a and b. The 50wt% CuO/CNT catalyst has a surface area of 72 m^2g^{-1} and has nanotubes wrapped around smooth oxide particles from 25-400nm in size and is shown in Figures S2c and d.

The electrochemical activity of the five catalysts is compared. The best performers for the cathodic and anodic cycles are the 50wt% MnO_2/CNT catalyst and the 50wt% NiO/CNT catalyst, respectively. The poorest performer of this series is the 50wt% Fe_xO_y/CNT catalyst. The ORR and OER are shown in Figures 8a and b, respectively. It was determined that the 50wt% MnO_2/CNT catalyst is the most active for ORR with a half wave potential of 0.84 V at the current density of -2.1 mA cm^{-2}. The 50wt% NiO/CNT catalyst is the most active for OER with an onset potential at 1.45V versus RHE.

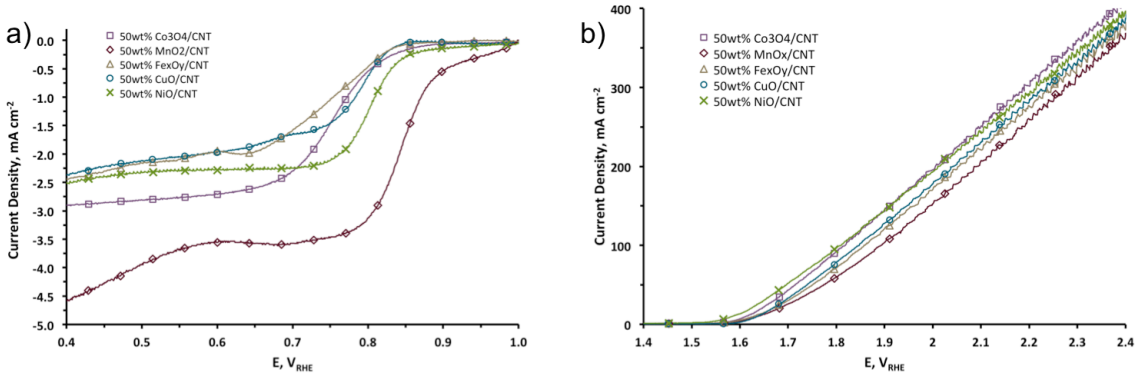

Figure 8. Electrochemical data for 50wt% MO_x/CNT (M: Co, Mn, Fe, Cu, Ni) catalysts, a) ORR and b) OER. Conditions: catalyst loading is 200µg cm^{-2}, 1M KOH, 1600RPM, 10mV s^{-1}.

Typically, state-of-the-art OER catalysts are unsupported materials due to the degradation of carbon during the reduction mechanisms. A durability study was conducted with the 50wt% NiO/CNT catalyst and it was found that the catalyst electrochemically improves after 1000 cycles, as illustrated in Figure 9 indicating minimal catalytic deterioration. Furthermore, the electrolyte was still clear after the durability test, representative of minimal residual amorphous carbon in the catalyst.

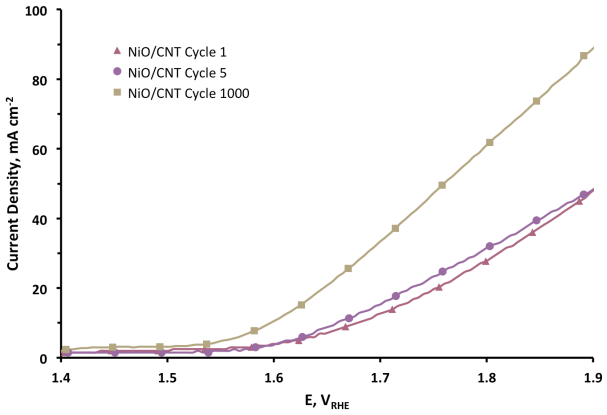

Figure 9. Electrochemical durability OER data for 50wt% NiO/CNT catalyst. Conditions: catalyst loading is 200μg cm^{-2}, 1M KOH, 1600RPM, 10mV s^{-1}.

From this series of 50wt% MO_x/CNT catalysts, the most active catalyst for ORR is the 50wt% MnO_2/CNT catalyst and the most active for OER is the 50wt% NiO/CNT catalyst. The inherent chemical properties of the catalyst provide promising electrochemical results.

Due to the nano-sized nature of the materials, the synthesis of a 25wt% NiO + 25wt% MnO_2/CNT catalyst was attempted. The results of this new catalyst have been electrochemically evaluated; however, for the purposes of this thesis, this material will be labeled "25wt% Ni + 25wt% Mn/CNT" since the oxide species present are still unknown. Chemical characterization is ongoing. During the ORR, the half-wave potential decreased

due to the drop in the limiting current by approximately 1 mA cm^{-2} as shown in Figure 10 and there is no electrochemical improvement for the ORR. The half-wave potential of the 25wt% Ni + 25wt% Mn/CNT is 0.80V with a limiting current density of -5.48 mA cm^{-2}. It is compared to the 50wt% MnO_2/CNT catalyst with a half-wave potential of 0.84 V.

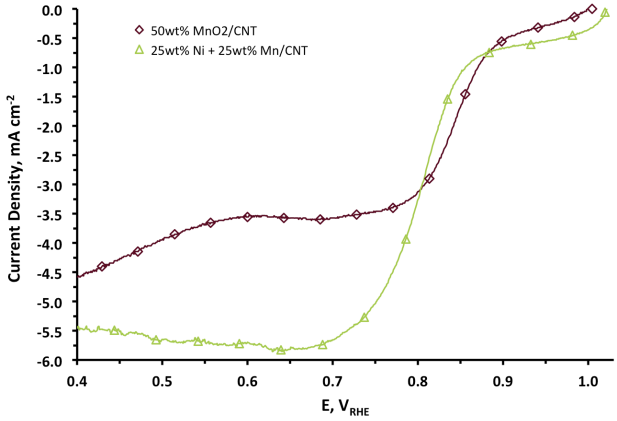

Figure 10. ORR electrochemical data for 50wt% MnO_2/CNT and 25wt% Ni +25wt% Mn/CNT. Conditions: catalyst loading is 200µg cm^{-2}, 1M KOH, 1600RPM, 10mV s^{-1}.

The bi-functional 25wt% Ni + 25wt% Mn/CNT catalyst shows improvement in the OER with an onset of 1.41 V in comparison to the 50wt% NiO/CNT catalyst that has an onset potential of 1.45 V vs. RHE. The results are shown in Figure 11.

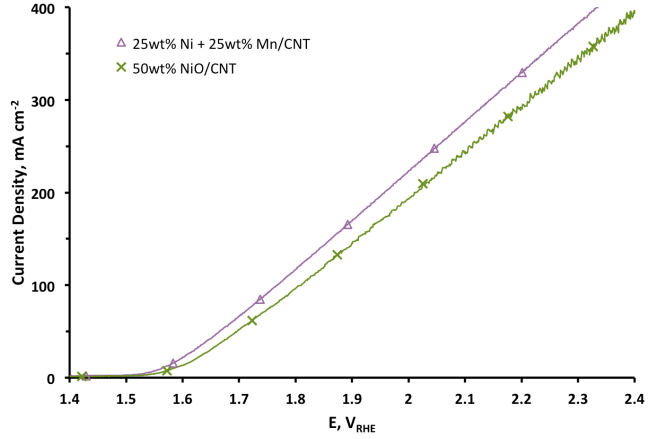

Figure 11. OER electrochemical data for 50wt% MnO_2/CNT and 25wt% Ni+25wt% Mn/CNT. Conditions: catalyst loading is 200µg cm^{-2}, 1M KOH, 1600RPM, 10mV s^{-1}.

From these electrochemical results, it is hypothesized that the addition of manganese oxides to a NiO/CNT catalyst is beneficial. This 25wt% Ni + 25wt% Mn/CNT catalyst has been physically analyzed by SEM as shown in Figure 12.

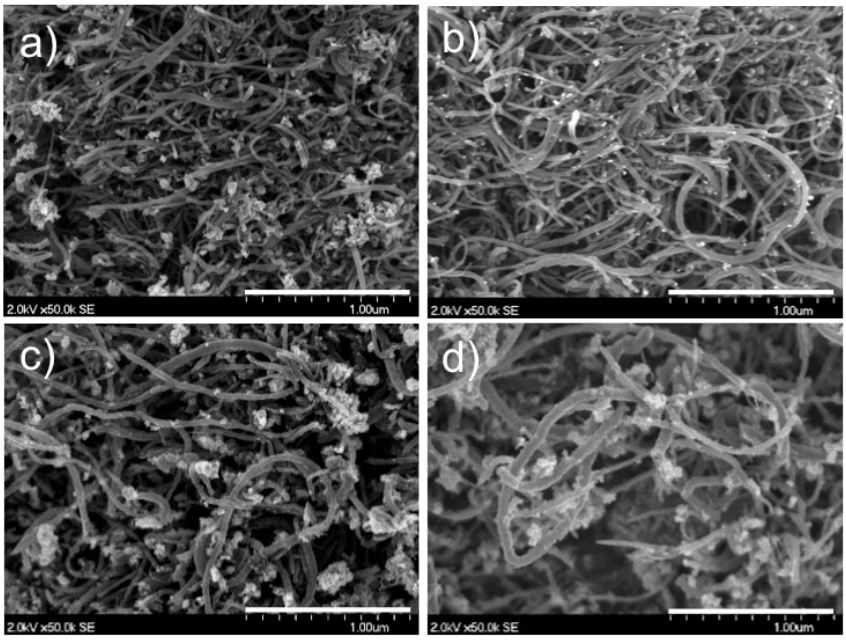

Figure 12. SEM images of a) 50wt% MnO_2/CNT, b) 50wt% NiO/CNT, c) and d) 25wt% Ni + 25wt% Mn/CNT catalyst.

From SEM analysis, the Ni and Mn oxide species deposited onto the nanotubes are widely dispersed and have porous characteristics. Further oxide loadings needs to be studied to understand these effects. By understanding the morphology of what makes catalysts different and comparing this to their electrochemical data, one can gain insight as to the particle size, shape and distribution that dictates an active catalyst from one that is deficient.

4.5 Conclusions

A method was developed in which high purity CNTs can be produced in large quantities with minimal amorphous carbon. There was successful deposition of the transition metal

oxides on the surfaces of the CNT catalysts. This research uncovers morphological insight into the characteristic qualities that determine a highly active catalyst. The electrochemical characteristics from the RDE experimentation show that the catalysts are bi-functionally active and can act as a replacement for conventional PGM-based catalysts in the appropriate conditions.

4.6 Supplementary Figures

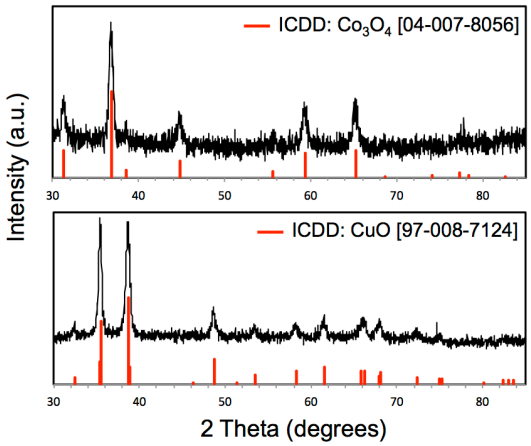

Figure S1. XRD data for a) 50wt% Co_3O_4/CNT and b) 50wt% NiO/CNT.

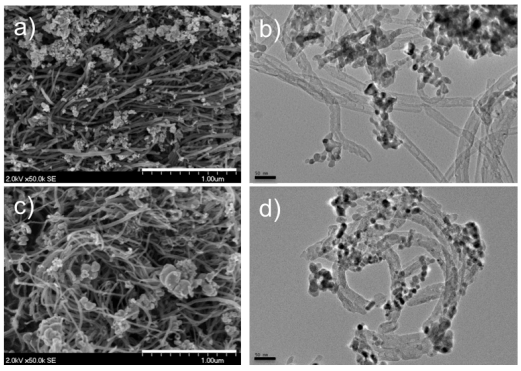

Figure S2. SEM (left column) and TEM (right column) of: a) and b) 50wt% Co_3O_4/CNT and c) and d) 50wt% CuO/CNT.

CHAPTER 5 RESEARCH OBJECTIVE 3: FURTHER CATALYST ELECTROCHEMICAL EVALUATION

From this research, the best catalysts are the $CuCo_2O_4$-SSM, 50wt% MnO_2/CNT and 25wt% Ni + 25wt% Mn/CNT catalysts. A further study was conducted to evaluate both the synthetic methods and chemical components comprising these three materials. The functionalized CNTs were further evaluated and an attempt was made to deposit the $CuCo_2O_4$ spinel on them. The sacrificial support method was utilized to study its effects with Ni and Mn oxide species.

5.1 MO_x/CNT Study with $CuCo_2O_4$

From the exploration of the $CuCo_2O_4$ spinel series and the success of the MO_x/CNT catalysts, further studies were conducted. An attempt was made to synthesize a $CuCo_2O_4$/CNT composite in which 25wt% of the spinel would be deposited onto the functionalized nanotubes. Following the same procedures as described in Section 4.3, Cu and Co nitrates were deposited onto CNTs and calcined at three different temperatures. The calcination temperature for the catalysts are 350°C, 400°C and 450°C for 180 minutes, and the three catalysts from this experiment are electrochemically compared. They are referred to as "25wt% Cu and Co/CNT" catalysts because the oxides have not been characterized by XRD. The best performer for ORR is the catalyst calcined at 350°C, with a half-wave potential of 0.83 V and a limiting current density of -4.4 mA cm^{-2} as shown in Figure 12 below.

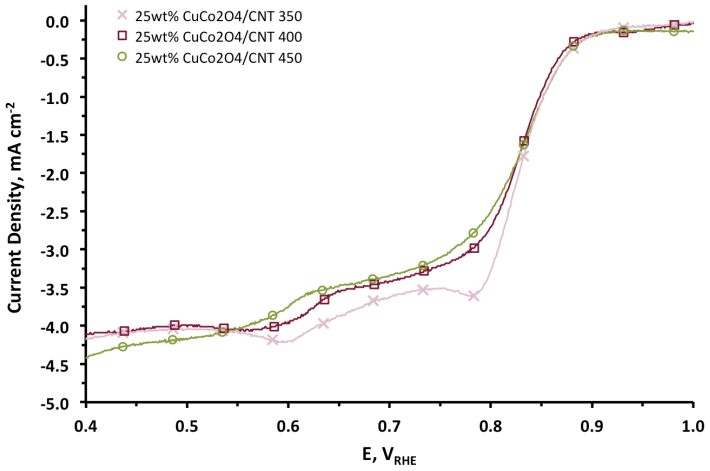

Figure 12. ORR electrochemical data for 25wt% Cu and Co/CNT calcined at 350°C, 400°C and 450°C. Conditions: catalyst loading is 400µg cm^{-2}, 1M KOH, 1600RPM, 10mV s^{-1}.

From the electrochemical data of the 25wt% Cu and Co/CNT 350°C catalyst, at 0.8 V and again at 0.6 V, it is hypothesized that the catalyst reactivates due to the slight increases in the current density. Since the current density increases at 0.6 V, and doesn't reach an equilibrium state at 0.4 V, the catalyst is not oxygen saturated at this point. The OER activity is shown below in Figure 13. The catalyst with the quickest onset potential of 1.49 V vs. RHE is the 25wt% Cu and Co/CNT catalyst calcined at 450°C.

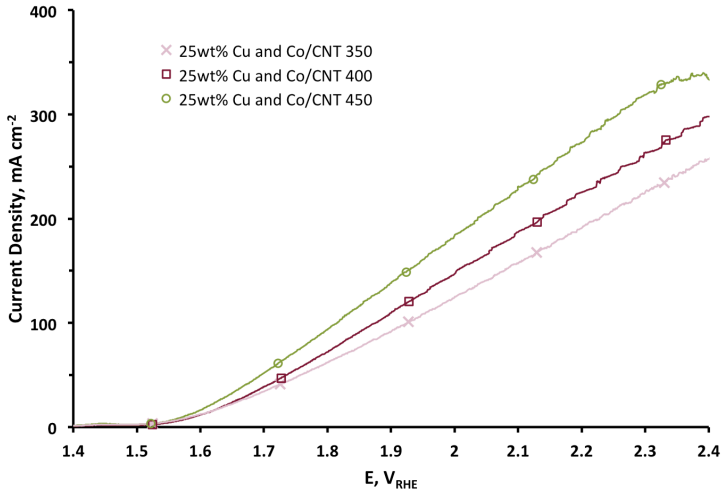

Figure 13. OER electrochemical data for 25wt% Cu and Co/CNT calcined at 350°C, 400°C and 450°C. Conditions: catalyst loading is 400µg cm^{-2}, 1M KOH, 1600RPM, 10mV s^{-1}.

The materials produced are bi-functionally active, although the species produced are not spinels. Spinels form at a temperature above 500°C. If the CNTs were exposed to a temperature higher than 450°C, then they would degrade into amorphous carbon. Despite not being able to synthesize a $CuCo_2O_4$/CNT composite, successful deposition of copper oxide and cobalt oxide species resulted in an electrochemically active catalyst. This further confirms the hypothesis that at least two catalytic components are necessary for successful bi-functional activity when compared to the results from Figure 8, showing ORR and OER of 50wt% Co_3O_4/CNT and 50wt% CuO/CNT. The catalyst loadings of the 50wt% Co_3O_4/CNT and 50wt% CuO/CNT catalysts were 200μg cm^{-2} versus the catalyst loading of 400μg cm^{-2} for the 25wt% Cu and Co/CNT catalysts, so the two cannot be directly compared. It can be deduced; however, from Figures 10 and 11 that the deposition of multiple transition metal oxides onto the surfaces of these functionalized CNTs yield positive electrochemical results.

5.2 SSM Study with Ni and Mn Oxides

The success of the deposition of the Ni and Mn oxides onto the surfaces of the CNTs, coupled with the high activity of the SSM $CuCo_2O_4$ spinel led to further experimentation. A study was conducted to see how the SSM synthesis procedure affected the activity of Ni and Mn species. Perovskites and spinels were synthesized based on Ni and Mn following the procedures described in Section 3.3 for the SSM catalyst. Six catalysts resulted: SSM NiO, SSM MnO_2, SSM $NiMn_2O_4$, SSM $MnNi_2O_4$, SSM $NiMnO_3$ and SSM $MnNiO_3$. The best ORR catalyst is the SSM MnO_2 catalyst, which has a half-wave potential of 0.66 V and a limiting current density of -1.44 mA cm^{-2} and shown in Figure 14. These catalysts cannot electrochemically compete with the other catalysts created, but they do provide bi-functional catalyst characteristics. It has been determined that

although the Ni and Mn oxides contribute to active catalysts, they do require carbon to increase their conductivity.

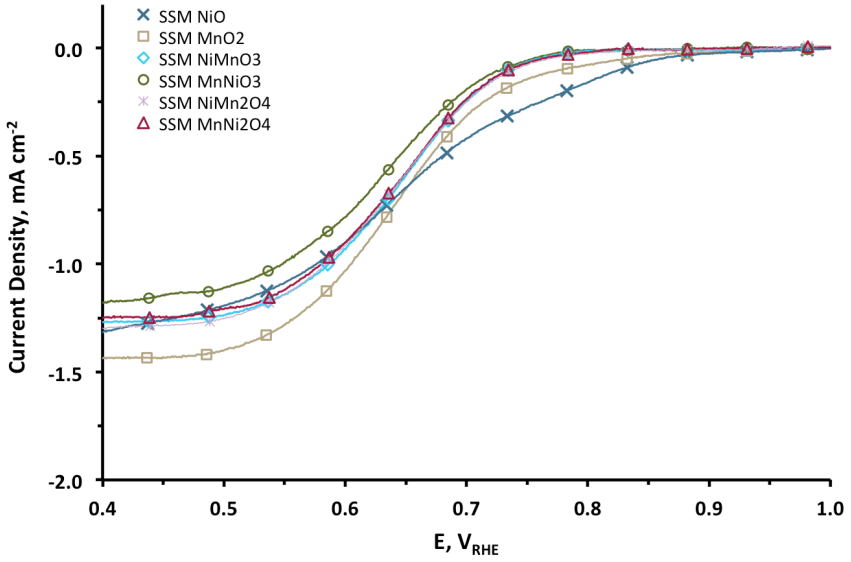

Figure 14. ORR electrochemical data for SSM NiO, SSM MnO_2, SSM $NiMnO_3$, SSM $MnNiO_3$, SSM $NiMn_2O_4$ and SSM $MnNi_2O_4$. Conditions: catalyst loading is 200µg cm^{-2}, 1M KOH, 1600RPM, 10mV s^{-1}.

The electrochemical results for the OER show that the SSM $NiMnO_3$ catalyst is the best performer with an onset potential of 1.56 V vs. RHE. This is shown in Figure 15.

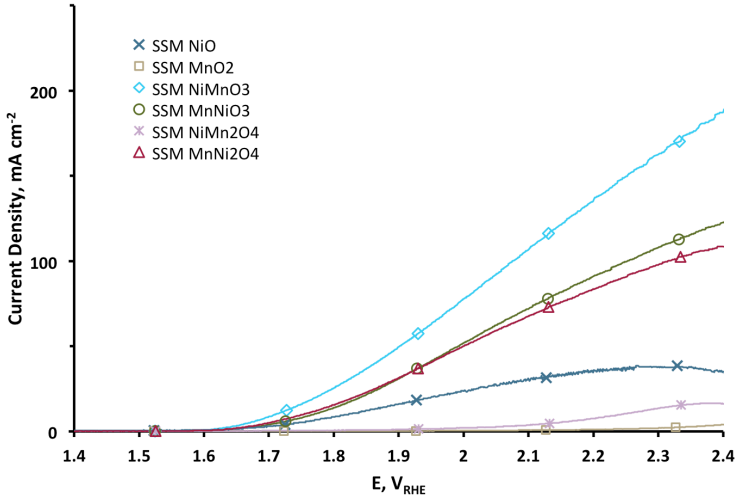

Figure 15. OER electrochemical data for SSM NiO, SSM MnO_2, SSM $NiMn_2O_4$, SSM $MnNi_2O_4$, SSM $NiMnO_3$ and SSM $MnNiO_3$. Conditions: catalyst loading is 200µg cm^{-2}, 1M KOH, 1600RPM, 10mV s^{-1}.

These results support the original notion that a mixture of Ni and Mn oxides yield higher OER activity than a single oxide specie like NiO or MnO_2. These results also support the trend found in Figure 11, where an addition of Mn oxide to Ni-based catalysts increases electrochemical activity. This data maintains the original hypothesis that for optimized bi-functionality, at least two oxide species should be present, *i.e.* have different oxidation states.

CHAPTER 6 SUMMARY

Twenty bi-functional catalysts were synthesized and characterized. This work extends the body of science around these catalysts. The properties measured place these materials among other comparable catalysts.

Studying the electrochemical activities and morphologies of several bi-functional catalysts has shed some light on the properties that make these materials function during the ORR and OER. From Chapter 3 and the exploration of $CuCo_2O_4$ spinel catalysts, it was found that the SSM synthesis technique yielded the most phase pure material in comparison to other synthetic approaches. The other three synthesis techniques resulted in traces of CuO (Figure 2). Since the $CuCo_2O_4$-SSM catalyst was the best performing of the series, it has been deduced that phase purity is necessary for good catalytic activity. This has been confirmed by the conductivity analyses of the four catalysts. The resistivity of the materials was evaluated and only the $CuCo_2O_4$-SSM catalyst was found to be conductive due to its small resistance of <1Ω. The catalytic activity is thus due to its phase purity and lack of CuO, which was found to have high electrical resistance of 400kΩ. The $CuCo_2O_4$-SSM shows active bi-functionality and is electrochemically more viable in comparison to the other three catalysts within this series.

Since carbon is known to be a good conductor, another series of catalysts were synthesized in which mixed metal oxides were deposited onto functionalized CNTs. From the work described in Chapter 4, transition metal oxide species could be successfully deposited onto CNTs. Furthermore, since the 50wt% NiO/CNT catalyst has the best OER activity (Figure 8b) and the 50wt% MnO_2/CNT catalyst has the best ORR

activity (Figure 8a), it has been hypothesized that it takes at least two separate components for a truly optimized bi-functional catalyst. The two metal oxides were combined to form a 25wt% Ni + 25wt% Mn/CNT catalyst. Although the specific oxide species on this material has not been evaluated, the electrochemical results show improved performance during the OER. A Ni-based catalyst designed for OER can benefit from the addition of a Mn-oxide specie.

Through further catalytic electrochemical evaluation, a study was conducted based on the findings from Chapters 3 and 4.

i) An effort was made to synthesize a 25wt% $CuCo_2O_4$/CNT catalyst; however, the calcination temperature of spinels is higher than the temperature at which CNTs can retain their structural integrity. Three materials were synthesized and calcined at temperatures of T=350°C, 400°C and 450°C. The mixture of Cu and Co oxide species on the CNTs yielded comparable electrochemical activity in correlation to the other catalysts presented in this thesis. These results confirm that if transition metal oxides are deposited onto CNTs for use as catalysis, having at least two oxide species enhances the activity.

ii) From the results of the 50wt% MnO_2/CNT and 50wt% NiO/CNT coupled with the SSM synthesis technique, pure oxides, spinels and perovskites were synthesized to evaluate the relationships between Mn and Ni and their bi-functional behaviors. It was found that the SSM MnO_2 catalyst had the highest ORR activity and the SSM $NiMnO_3$ catalyst has the best OER activity. These results verify the similar trend of the Ni and Mn oxide species from the CNT study (Figure 8a) and also support the hypothesis that for a material to be optimized bi-functionally, it needs to have at least two oxide species.

Furthermore, the OER activity of the SSM $NiMnO_3$ endorses the idea that a Ni-based oxide catalyst benefits from the addition of Mn. This study on SSM Ni and Mn materials has confirmed the necessity of carbon for Ni and Mn-based materials to provide for their conductivity. These results also allow for an appreciation of the SSM $CuCo_2O_4$ material for having such high activity with no additional carbon.

6.1 Conclusions

To complete the first two research objectives, two families of catalysts were synthesized: the first, a series of $CuCo_2O_4$ spinels and the second, a group of 50wt% MO_x/CNT catalysts. From the results of these studies, further experimentation ensued to synthesize spinels deposited on CNTs and SSM-derived spinels for the third research objective. After additional improvements, these catalysts can be used in real energy conversion systems. This research enabled an understanding of bi-functional catalyst characteristics. It is assumed that the ability for the same catalyst to perform well as an oxygen reducer and oxygen evolver lies in the relationship between the triple-phase boundaries between the components of the catalyst and its constituents and their relation to the electrolyte. In the first body of work, it was found that the $CuCo_2O_4$-SSM catalyst was the best performer with a half-wave potential of 0.80V with a limiting current density of -3.66 mA cm^{-2} and an onset potential of 1.52V versus RHE during the OER. In the second body of work, the 50wt% MnO_2/CNT catalyst was the best ORR catalyst with a half wave potential of 0.84V and the 25wt% Ni + 25wt% Mn/CNT catalyst was the best performer for OER with an onset potential of 1.41V versus RHE. Among all of the catalysts synthesized and electrochemically analyzed in this study, these two CNT-based catalysts were the most active.

The results of all synthesized catalysts are tabulated below in the order that they were presented. All catalysts were tested at 10 mV s^{-1} at 1600 RPM in 1.0M KOH. The most electrochemically active are highlighted.

Table 1. Total Catalyst ORR/OER Data

Location in Thesis	**Catalyst** loading: 200 μg cm^{-2} unless otherwise stated	**ORR**		**OER**
		Half-wave potential (V)	Limiting current density (mA cm^{-2})	Onset potential vs. RHE (V)
Ch. 3	$CuCo_2O_4$ – PF	0.76	-3.28	1.53
	$CuCo_2O_4$ – SG	0.75	-3.15	1.56
	$CuCo_2O_4$ – SP	0.75	-3.41	1.53
	$CuCo_2O_4$ – SSM	0.80	-3.66	1.52
	CuO - SSM	0.65	-1.24	1.60
Ch. 4	50wt% Co_3O_4/CNT	0.76	-2.90	1.53
	50wt% MnO_2/CNT	0.84	-4.56	1.53
	50wt% Fe_xO_y/CNT	0.75	-2.42	1.55
	50wt% CuO/CNT	0.76	-2.32	1.54
	50wt% NiO/CNT	0.80	-2.48	1.45
	25wt% Ni + 25wt% Mn/CNT	0.80	-5.48	1.41
Ch. 5.1	25wt% Cu + Co/CNT 350°C loading: 400 μg cm^{-2}	0.83	-4.40	1.50
	25wt% Cu + Co/CNT 400°C loading: 400 μg cm^{-2}	0.82	-4.10	1.51
	25wt% Cu + Co/CNT 450°C loading: 400 μg cm^{-2}	0.82	-4.10	1.49
Ch. 5.2	SSM NiO	0.65	-1.30	1.58
	SSM MnO_2	0.66	-1.44	1.71
	SSM $NiMnO_3$	0.65	-1.27	1.56
	SSM $MnNiO_3$	0.63	-1.17	1.58
	SSM $NiMn_2O_4$	0.65	-1.29	1.66
	SSM $MnNi_2O_4$	0.65	-1.24	1.58

6.2 References

[1] J. Greeley, I. E. L. Stephens, A. S. Bondarenko, T. P. Johansson, H. A. Hansen, T. F. Jaramillo, J. Rossmeisl, I. Chorkendorff and J. K. Nørskov. *Nature Chem*. **2009**, 1, 552–556.

[2] T. Reier, M. Oezaslan and P. Strasser. *ACS Catal.* **2012**, 2 (8), 1765-1772.

[3] Ø. Ulleberg. *Int. J. Hydrogen Energy.* **2003**, 28 (1), 21-33.

[4] J-S. Lee, S. T. Kim, R. Cao, N-S. Choi, M. Liu, K. T. Lee, J. Cho. *Adv. Energy Mater.* **2011**, 1 (1), 34–50.

[5] DOE Energy Efficiency & Renewable Energy: Fuel Cells. Retrieved November 7, 2013. [http://www1.eere.energy.gov/hydrogenandfuelcells/fuelcells/fc_types.html].

[6] Kinoshita, K. (1992) *Electrochemical Oxygen Technology*. New York: John Wiley & Sons.

[7] K. M. Abraham, Z. Jiang. *J. Electrochem. Soc*. **1996**, 143 (1), 1-5.

[8] T. Ogasawara, A. Débart, M. Holzapfel, P. Novák, P. G. Bruce. *J. Am. Chem. Soc*. **2006**, 128 (4), 1390-1393.

[9] NASA Space Applications of Hydrogen and Fuel Cells. Retrieved November 8, 2013. [http://www.nasa.gov/topics/technology/hydrogen/hydrogen_2009.html]

[10] Dr. Benjamin Levich. (1962) *Physicochemical Hydrodynamics.* Prentice Hall.

[11] Pine Instruments. Retrieved November 7, 2013. [http://www.pineinst.com/echem/productsubcats.asp?categoryID=1]

[12] A. Serov, U. Martinez, A. Falase, P. Atanassov, *Electrochem. Comm.* **2012**, 22,193-196.

[13] Y. Shimizu, K. Uemura, H. Matsuda, N. Miura, N. Yamazoe. *J. Electrochem. Soc*. **1990**, 137 (11), 3430-3433.

[14] C. Jin, X. Cao, L. Zhang, C. Zhang, R. Yang. *J. Power Sources.* **2013**, 241, 225-230.

[15] Z. Chen, A. Yu, D. Higgins, H. Li, H. Wang, Z. Chen. *Nano Lett.* **2012**, 12, 1946-1952.

[16] X. Wu, K. Scott. *J. Power Sources*. **2012**, 206, 14-19.

[17] L. Wang, X. Xhao, Y. Lu, M. Xu, D. Zhang, R. S. Ruoff, K. J. Stevenson, J. B. Goodenough. *J. Electrochemical Soc.* **2011**, 158 (12), A1379-A1382.

[18] E. Antolini. *Appl. Catal., B* **2009**, 88, 1-24.

[19] Y-C. Lu, Z. Xu, H.A. Gasteiger, S. Chen, K. Hamad-Schifferli, Y. Shao-Horn. *J. Am. Chem. Soc.* **2010**, 132, 12170-12171.

[20] Y. Shimizu, K. Uemura, H. Matsuda, N. Miura, N. Yamazoe. *J. Electrochem. Soc.* **1990**, 137, 11, 3430-3433.

[21] O. Haas, F. Holzer, S. Müller, J.M. McBreen, X.Q. Yang, X. Sun, M. Balasubramanian. *Electrochim. Acta.* **2002**, 47, 3211-3217.

[22] X. Wang, P.J. Sebastian, M.A. Smit, H. Yang, S.A. Gamboa. *J. Power Sources.* **2003**, 124, 278-284.

[23] S. Velraj, J.H. Zhu. *J. Power Sources.* **2013**, 227, 48-52.

[24] Z. Chen, A. Yu, D. Higgins, H. Li, H. Wang, Z. Chen. *Nano Lett.* **2012**, 12, 1946-1952.

[25] W. Yang, J. Salim, S. Li, C. Sun, L. Chen, J.B. Goodenough, Y. Kim. *J. Mater. Chem.* **2012**, 22, 18902-18907.

[26] W. Yang, J. Salim, C. Ma, Z. Ma, C. Sun, J. Li, L. Chen, Y. Kim. *Electrochem. Commun.* **2013**, 28, 13-16.

[27] L. Wang, M. Ara, K. Wadumesthrige, S. Salley, K.Y.S. Ng, *J. Power Sources* **2013**, 234, 8-15.

[28] Y. Zhao, L. Xu, L. Mai, C. Han, Q. An, X. Xu, X. Liu, Q. Zhang, *Proc. Natl. Acad. Sci.* **2012**, 109, 48, 19569-19574.

[29] S. Pylypenko, S. Mukherjee, T. S. Olson, P. Atanassov. *Electrochim. Acta*. **2008**, 53, 7875-7883.

[30] M. H. Robson, A. Serov, K. Artyushkova, P. Atanassov. *Electrochim. Acta*. **2013**, 90, 656–665.

[31] S. Brocato, A. Serov, P. Atanassov, *Electrochim. Acta*. **2013**, 87, 361-365.

[32] A. Serov, M. H. Robson, K. Artyushkova, P. Atanassov. *Appl. Catal. B*. **2012**, 127, 300-306.

[33] A. Serov, M. H. Robson, M. Smolnik, P. Atanassov, *Electrochim. Acta.* **2012**, 80, 213-218.

[34] A. Serov, M. H. Robson, B. Halevi, K. Artyushkova, P. Atanassov. *Electrochem. Comm*. **2012**, 22, 53-56.

[35] A. Falase, M. Main, K. Garcia, A. Serov, C. Lau, P. Atanassov. *Electrochim. Acta*. **2012**, 66, 295-301.

[36] A. Serov, U. Martinez, P. Atanassov. Electrochem. Comm. 34 (2013) 185-188.

[37] A. Serov, M. H. Robson, M. Smolnik, P. Atanassov. *Electrochim. Acta.* **2013**, 109, 433-439.

[38] A. Serov, U. Martinez, A. Falase, P. Atanassov, *Electrochem. Comm.* **2012**, 22, 193-196.

[39] S. Pylypenko, S. Mukherjee, T. Olson, *Electrochim. Acta.* **2008**, 53, 7875-7883.

[40] A. Serov, M.H. Robson, B. Halevi, K. Artyushkova, P. Atanassov, *Electrochem. Comm.* **2012**, 22, 53-56.

[41] A. Serov, M.H. Robson, M. Smolnik, P. Atanassov. *Electrochim. Acta.* **2012**, 80, 213-218.

[42] A. Serov, M.H. Robson, K. Artyushkova, P. Atanassov. *Appl. Catal., B.* **2012**, 127, 300-306.

[43] H.A. Gasteiger, S.S. Kocha, B. Sompalli, F.T. Wagner,.*Appl. Catal., B.* **2005**, 56, 9-35.